RSC Advances

PAPER

View Article Online
View Journal | View Issue

Cite this: *RSC Adv.*, 2015, **5**, 665

Poor solvent and thermal annealing induced ordered crystallites in poly(3-dodecylthiophene) films†

I. Roy and S. Hazra*

Received 17th September 2014
Accepted 7th November 2014

DOI: 10.1039/c4ra10629f

www.rsc.org/advances

The influence of poor solvent and thermal annealing, and their specific roles, in the crystalline ordering of poly(3-dodecylthiophene) [P3DDT] films, which are of immense importance in their performance as semiconducting materials, were investigated using complementary techniques. Edge-on oriented crystallites (Form-II like) are enhanced in the as-cast films prepared after addition of a poor solvent. However, the coil-to-rod-like conformational transition is more prevalent compared to the crystallites, suggesting that a poor solvent predominantly helps to overcome the unfavorable conformational transition. A very large enhancement in the amount of the crystallites (Form-I-like) is observed for the films annealed above the melting temperature of the alkyl side chains, suggesting thermal annealing essentially helps to promote the diffusion of rod-like chains and to overcome the hindrance of the π–π stacking. Perfectly edge-on oriented crystallites, which are enhanced with increasing annealing temperature, start to deteriorate when the melting temperature of the polymer backbone is reached. The domain-like morphology of the as-cast film, however, remains almost unchanged upon thermal annealing suggesting the spontaneous organization of π-stacked layers through alkyl side chains to form crystallites is essentially within the small domains. The best edge-on oriented crystallites are found for the P3DDT films prepared from a solution containing a large amount of poor solvent and subsequently annealing the film at around 130 °C.

1 Introduction

In recent years semiconducting polymers have been widely used for the fabrication of organic electronic devices like organic light-emitting diodes (OLEDs),[1,2] polymer solar cells (PSCs)[3,4] and thin film transistors (TFTs).[5,6] In this regard poly(3-alkylthiophenes) (P3ATs), belonging to the large class of π-conjugated polymers, have gained extreme importance due to their availability, easy processing techniques and high charge carrier mobility.[5,7,8] Their high conjugation length endows them with high charge carrier mobility, whereas the flexible long alkyl side chains attached to their stiff backbones make them easily soluble in common organic solvents,[9,10] which is why they are suitable for the fabrication of photovoltaic devices using simple solution processing techniques.[11] The chemical incompatibility between the π-conjugated polythiophene backbone and the alkyl side chains gives rise to a lamellar structure (as shown in Fig. 1) containing alternate layers of polythiophene backbones and alkyl chains.[12] The semi-crystalline nature of P3AT results from the presence of such lamellar regions along with amorphous interlamellar regions. The lamellae can adopt two possible orientations on a substrate – the edge-on and the face-on orientations. The orientation and ordering in P3AT films greatly influence their performance as semiconducting materials, as the field-effect mobilities of devices strongly depend on them. The orientation and ordering can be influenced by various factors such as regioregularity and molecular weight,[7,13] length of alkyl side chain,[14] the solvent from which the film is cast,[15] nature of the substrate[16] and deposition technique used, such as drop-casting, spin-coating, dip-coating and directional epitaxial crystallization.[17–20]

Different approaches have been taken to increase the crystallinity and control the morphology and microstructure of P3AT films, such as optimization of the processing parameters, thermal annealing, solvent vapour treatment, *etc.*[21] A relatively simple method for preparing 1D aggregates of P3ATs was proposed by Kiriy *et al.*[22] This method suggests that by adding a poor solvent one can induce ordered main chain collapse of the P3AT molecules, resulting in the formation of 1D aggregates driven by solvophobic interactions. A poor solvent having lower volatility than the main solvent resides within the evolving film for a longer time during solvent evaporation, thus aiding in the growth of ordered aggregates.[23] 2D single crystalline nanosheets of P3HT were prepared by Yu *et al.* using slow evaporation of a diluted mixture of solvents.[24] It was shown that the ratio of good

Saha Institute of Nuclear Physics, 1/AF Bidhannagar, Kolkata 700064, India. E-mail: satyajit.hazra@saha.ac.in

† Electronic supplementary information (ESI) available. See DOI: 10.1039/c4ra10629f

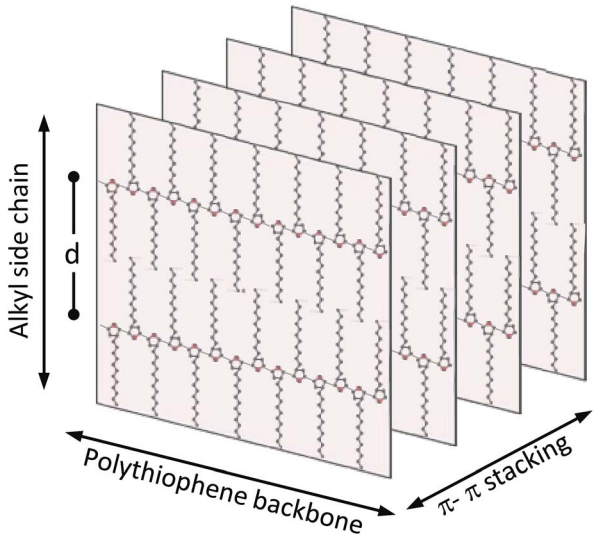

Fig. 1 Schematic of the P3AT crystallite structure, showing the π–π stacking, the polythiophene backbone (or conjugation) and alkyl side chain directions, and also the separation (*d*) between alternate layers of polythiophene backbones along the alkyl side chains.

solvent to poor solvent can control the size of the nanostructures. Later on, Chang *et al.* showed that a high volatility solvent can also lead to enhanced supramolecular assembly if it interacts with the main solvent through hydrogen bonding.[25] However, not much has been studied about poly(3-dodecylthiphene) (P3DDT) which has the longest alkyl side chain among the P3ATs. The longer side chain is responsible for its better solubility, but hinders its crystallizability due to side chain interactions. Because of this P3DDT tends to crystallize into spherulites and not nanowhiskers. Xu *et al.* reported the successful formation of P3DDT nanowhiskers by the addition of anisole, a poor solvent for P3DDT, to a solution of P3DDT in chlorobenzene or carbon disulfide, which are good solvents for the polymer.[26] In this case the crystallites or aggregates were prepared by heating the mixed solution and subsequently cooling and aging the solution, like others. However, no attempt has been made to study the P3DDT films prepared from solutions of different good solvent to poor solvent ratios both without heating and with subsequent annealing of the films at different temperatures to understand the definite roles of mixed solvent and annealing temperature on the structures of the P3DDT films. Such an understanding will definitely help us to prepare P3DDT films with structures that have potential to show better device properties.

In this paper, we have tried to understand exactly the role of the poor solvent and annealing temperature on the structures of the P3DDT films using complementary techniques. For this purpose, P3DDT films were first prepared from solutions containing different chlorobenzene-to-anisole ratios without heating and then subsequently annealed at different temperatures, and studied using X-ray diffraction (XRD), grazing incidence X-ray scattering (GISAXS), atomic force microscopy (AFM) and ultraviolet-visible (UV-vis) spectroscopy. Enhancement of rod-like conformation of chains in the films with an increasing proportion of the poor solvent, due to the coil-to-rod transition, is clearly evident. Such rod-like chains, which are mostly free or random in the as-cast films, are found to organize to form lamellae or crystallites upon thermal annealing. Simple XRD mapping helps us to find the optimum annealing temperature at which the maximum amount and/or size of highly edge-on oriented lamellae are formed, which is of great importance.

2 Experimental

Regioregular poly(3-dodecylthiophene) (P3DDT) was purchased from Sigma-Aldrich (average molecular weight: 60 000; regioregularity ≥ 98.5%) and used as received. Chlorobenzene (CB) and anisole (AN) were obtained from Sigma-Aldrich. P3DDT was first dissolved in CB, and then AN was added to the solution such that the concentration of the final solution was 0.25 mg ml^{-1}. CB and AN were mixed in the volume ratios 1 : 4, 1 : 7 and 1 : 11. Films were prepared by drop-casting the solutions after about 4 h (as the majority of the conversion takes place within that time according to the literature,[26] which is also shown in Fig. S1†) onto solid substrates and through slow evaporation (by keeping the solutions inside Petri dishes). The films deposited on the Si substrates from the three solutions are referred to as 1 : 4 CB–AN, 1 : 7 CB–AN and 1 : 11 CB–AN. To check the effect of the nature of the Si surface on the film structure, films were deposited on differently passivated [O- and H-] and oriented [(001) and (111)] Si substrates. O- and H-passivated Si substrates were prepared through pretreatment as reported before.[27–30] To compare the effect of mixed solvent with respect to the single solvent CB, films were also prepared on Si substrates from a solution of P3DDT in CB. For the optical study, 1 : 11 CB–AN films were deposited on clean quartz glass substrates. Thermal annealing of the films was done by placing the samples covered in glass Petri dishes in a box furnace. For the annealing at different temperatures, different films were generally used. For comparison, a single 1 : 11 CB–AN film deposited on glass substrate was also annealed at different temperatures.

XRD measurements of the films were performed on a versatile X-ray diffractometer (VXRD) setup.[31,32] VXRD consists of a diffractometer (D8 Discover, Bruker AXS) with a Cu source (sealed tube) followed by a Göbel mirror to select and enhance Cu Kα radiation ($\lambda = 1.54$ Å). The diffractometer has a two-circle goniometer [$\theta(\omega) - 2\theta$] with a quarter-circle Eulerian cradle as the sample stage. The latter has two circular (χ and ϕ) and three translational (X, Y, and Z) motions. The scattered beam was detected using a NaI scintillation (point) detector. Initially, conventional XRD measurements (*i.e.* θ–2θ scan)[31] were carried out for the as-cast, 60 °C-annealed and 165 °C-annealed 1 : 4 CB–AN, 1 : 7 CB–AN and 1 : 11 CB–AN films and also for the films deposited on glass substrates and annealed at different temperatures. Later, rocking (θ) scans[33] around the intense Bragg peak ($2\theta_B$) were carried out for one set of mixed-solvent (1 : 11 CB–AN) films and one set of single-solvent (CB) films, annealed at different temperatures. Subsequently, XRD measurements for different offset angles $\Delta\theta$ with respect to the peak position (θ_P) of the rocking curve, were also carried out for

This journal is © The Royal Society of Chemistry 2015

those samples. These scans can be used to generate two-dimensional XRD maps.

GISAXS measurements of the as-cast, 60 °C-annealed and 165 °C-annealed 1 : 4 CB–AN, 1 : 7 CB–AN and 1 : 11 CB–AN films were carried out using a synchrotron source (P03 beam line, PETRA III)[34–36] at an energy of 13 keV. The scattered beam was detected using a 2D detector (PILATUS 300k, Dectris, having 487 × 619 pixels of pixel size 172 μm). The sample-to-detector distances for the as-cast and annealed samples were 1005 and 1721 mm, respectively. For data collection, the incident angle α was kept at 0.4° and 0.25° for the as-cast and annealed samples, respectively. The direct beam was stopped and the specular reflected beam was attenuated by two separate point-like beam stops to avoid the saturation of the detector.

The top surface morphologies of the as-cast, 130 °C-annealed and 165 °C-annealed 1 : 11 CB–AN P3DDT films on Si substrates were mapped through AFM (beam deflection AFM, Omicron NanoTechnology)[29,32] on different length scales (0.2–7 μm). AFM images were collected in noncontact mode and in UHV ($\sim 10^{-10}$ mbar) conditions. Optical absorption spectra of the 1 : 11 CB–AN P3DDT films on quartz substrates after annealing at different temperatures were collected using a UV-vis spectrophotometer (Perkin Elmer, Lambda 750). For comparison, UV-vis spectra of P3DDT solutions prepared using single (CB) and mixed (CB–AN) solvents were also collected. For the estimation of the size and/or conformation/structure of the P3DDT molecules/aggregates, dynamic light scattering (DLS) measurements (Zetasizer Nano-S, Malvern Instrument) were performed for the solutions.

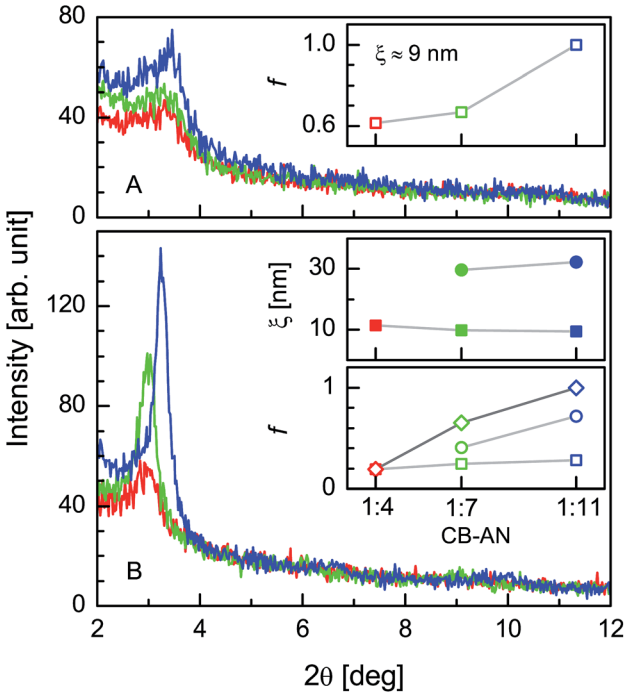

Fig. 2 XRD data (red, green and blue) of the as-cast (A) and 165 °C-annealed (B) 1 : 4, 1 : 7 and 1 : 11 CB–AN P3DDT films, showing a Bragg peak due to the alternate layers of polythiophene backbones along the alkyl side chains. Insets: corresponding variation of crystallite size (ξ) and relative amount (f) with solvent ratio.

3 Results and discussion

3.1 Structure from X-ray diffraction

3.1.1 Influence of poor solvent and optimization. In this section, the influence of poor solvent on the structures (*i.e.* the amount, size and orientation of the crystallites) of P3DDT films with and without thermal annealing, as observed from the conventional XRD and GISAXS measurements, will be presented to determine the best good solvent to poor solvent ratio. Thermal annealing was carried out at 60 and 165 °C, which are above the two endothermic peaks corresponding to the melting of the alkyl side chains and polythiophene backbones observed in the DSC thermogram of the P3DDT powder (shown in Fig. S2†).[37,38] The XRD data of the 1 : 4, 1 : 7 and 1 : 11 CB–AN samples are shown in Fig. 2. The peak at around 3.3°, corresponding to the separation (d) between alternate layers of polythiophene backbones along the alkyl side chains (as shown in Fig. 1) is observed in all the curves, indicating the presence of small crystallites of P3DDT molecules with predominantly edge-on orientations. The position, width and intensity of this peak vary, however, indicating change in the d-spacing, size and amount of crystallites. For the as-cast films the position of the peak is almost the same but the intensity increases slightly with increasing proportion of the poor solvent. After annealing the films at 60 °C there is almost no change (apart from a very slight shift in the position of the peak) in the XRD curves (not shown here). Annealing the films at 165 °C results in a very large increase in the peak intensity and a slight decrease in the peak position. For the 1 : 11 CB–AN sample, the change in the intensity of the peak is the greatest, while the change in the position is the smallest. Similar behavior in the XRD patterns (see Fig. S3 of ESI†) is observed for the films deposited on the Si substrates with different passivations and orientations [such as O–Si(111), H–Si(111) or H–Si(001)] and thus needs no separate discussion.

To get quantitative information about the crystallinity of the films, each XRD data around the peak is fitted with single or double Gaussian peak(s) along with an exponentially decreasing background. The Bragg peaks of the as-cast films and the 165 °C-annealed 1 : 4 CB–AN film are well fitted with a single Gaussian peak, while those of the 165 °C-annealed 1 : 7 and 1 : 11 CB–AN films are fitted with two Gaussian peaks. The width of the Gaussian peak is used to estimate the crystallite size (ξ) using the standard Scherrer's formula

$$\xi = \frac{C\lambda}{\beta \cos \theta_B}$$

where C is a dimensionless Scherrer constant which depends on the shape of the crystallites, the (hkl) index of the diffraction peak and the instrumental factor and whose value is taken to be 0.9, λ is the wavelength of the X-ray, β is the full width at half maximum (FWHM in radians) and θ_B is the Bragg angle. The d-values estimated from the XRD peak positions are tabulated in Table 1. The crystallite size and normalized amount, estimated from the width and intensity of Gaussian peak(s), are plotted in

Table 1 *d*-value, size (ξ) and normalized amount (f) parameters for the P3DDT crystallites in the as-cast and annealed films prepared from different ratios of good solvent to poor solvent

	As-cast			165 °C-annealed					
Sample	*d*-value (nm)	ξ (nm)	f	*d*-value (nm)	ξ_1 (nm)	ξ_2 (nm)	f_1	f_2	f
1 : 4 CB–AN	2.66	9	0.6	2.98	11	—	0.2	—	0.2
1 : 7 CB–AN	2.66	9	0.7	2.96	10	30	0.2	0.4	0.6
1 : 11 CB–AN	2.65	9	1.0	2.72	9	32	0.3	0.7	1.0

the insets of Fig. 2 and also tabulated in Table 1. It is clear from the figure and the table that for the as-cast films, very small (~9 nm) sized crystallites having a *d*-value of 2.66 nm, are formed. The normalized amount of crystallites increases with increasing proportion of poor solvent from 0.6 to 1.0. For the 165 °C-annealed films the crystallite size and/or amount increases appreciably with increasing proportion of poor solvent. Relatively large (~30 nm) sized crystallites are also formed for the 1 : 7 and 1 : 11 CB–AN films, the amount of which is found to be greatest for the latter. The *d*-value was also found to increase with thermal annealing; this change was smallest for the 1 : 11 CB–AN films.

GISAXS patterns of the as-cast and 165 °C-annealed films are shown in Fig. 3. The presence of Bragg arcs corresponding to the separation between the alternate layers of polythiophene backbones along the alkyl side chains is clearly visible in all the patterns. The arc nature suggests that the predominantly edge-on oriented lamellae have some deviations as well. There is very little variation in the GISAXS patterns of the as-cast films. The nature remains almost the same for the 60 °C-annealed films (not shown here), while for the 165 °C-annealed films the Bragg arc intensity increases, slightly for 1 : 4 CB–AN film but greatly for 1 : 11 CB–AN film. To better understand the film structure, GISAXS line profiles along the q_z and q_y directions were generated from a vertical cut and a horizontal arc, respectively, through the Bragg spot (as shown in Fig. 3) and are plotted in Fig. 4. The GISAXS line profiles along the q_z direction (Fig. 4A and C) exactly follow the XRD data (Fig. 2), and hence provide the same information about the crystallites. The GISAXS line profiles along the q_y direction provide additional information about the orientation of the crystallites. Considering a Gaussian distribution, the angular spread in the orientation of the crystallites with respect to the perfect edge-on orientation is estimated from the FWHM. For the as-cast films, the crystallites are found within an angular spread of ±20°, with slightly enhanced probability within ±5°. For the 165 °C-annealed films, the angular spread decreases, being smallest for the 1 : 11 CB–AN film. For this film, the crystallites are found within an angular spread of ±12°, with strongly enhanced probability within ±5°.

It is clear from both the XRD and GISAXS results that there is a very large difference in crystallinity among the 165 °C-annealed films, although very little difference is observed among the as-cast films. Such apparently anomalous behavior can be understood by considering well known two step

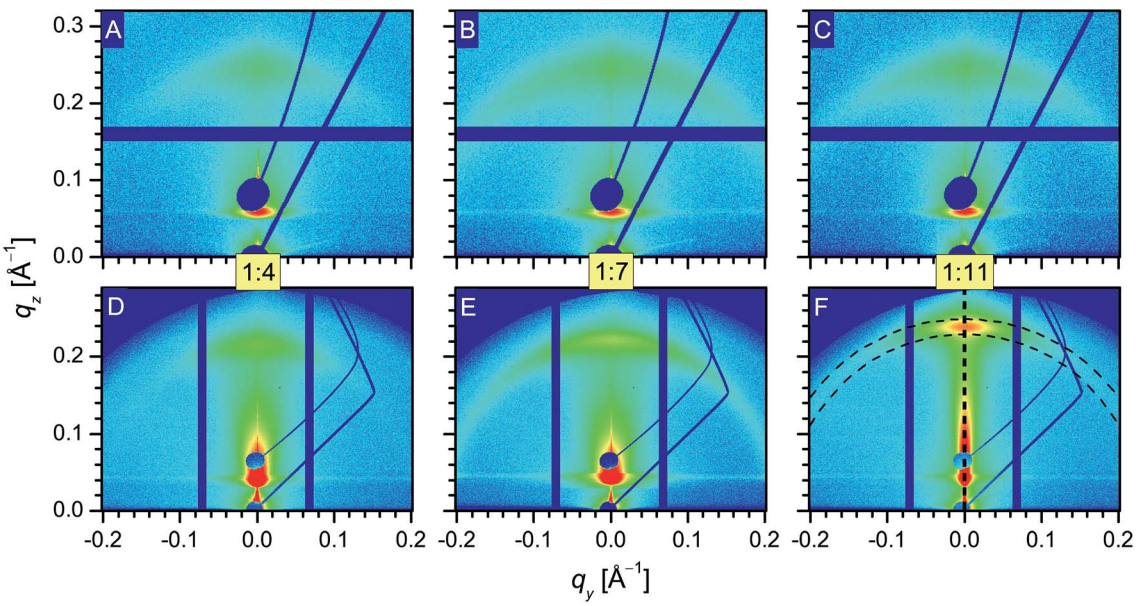

Fig. 3 GISAXS patterns of the as-cast (A, B and C) and 165 °C-annealed (D, E and F) 1 : 4, 1 : 7 and 1 : 11 CB–AN P3DDT films, showing Bragg arcs corresponding to the alternate layers of polythiophene backbones and alkyl side chains.

This journal is © The Royal Society of Chemistry 2015

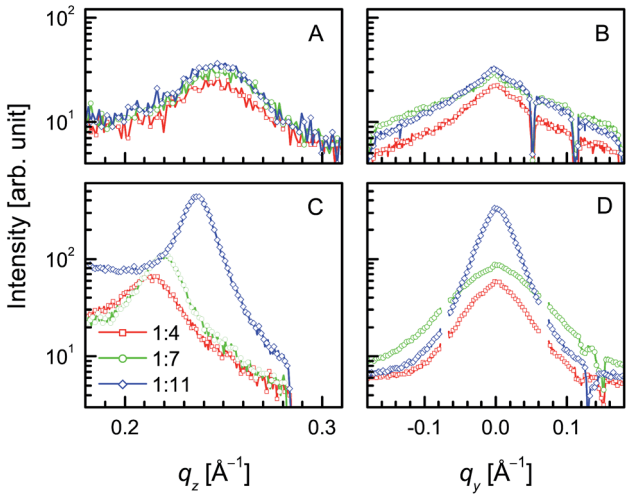

Fig. 4 GISAXS line profiles along the q_z (*i.e.* vertical cut through the Bragg spot) and q_y (*i.e.* horizontal arc through the Bragg spot) directions of the as-cast (A and B) and 165 °C-annealed (C and D) 1 : 4, 1 : 7 and 1 : 11 CB–AN P3DDT films.

processes, namely the coil-to-rod transformation of the polymers and the subsequent organization of the rods to form crystallites. The coil-to-rod transformation is enhanced with increasing proportion of poor solvent, while the subsequent organization of the rods to form nearly edge-on oriented lamellae is enhanced with increasing temperature. At room temperature, a few rods are probably organized to form very few small (~9 nm) size crystallites, which we could detect. At higher temperatures, the organization is enhanced, which tends to increase the amount and size of the crystallites. However, the initial number of rods, which act as nuclei, restricts the amount and size of the crystallites. Accordingly, few small (~11 nm) sized crystallites are found in the 1 : 4 CB–AN annealed film, while many large (about 32 nm) sized crystallites are found in the 1 : 11 CB–AN annealed film.

3.1.2 Influence and optimization of annealing temperature. In this section the influence of the annealing temperature on the structure (*i.e.* the amount, size and orientation of the crystallites) of the 1 : 11 CB–AN (optimum mixed solvent) film, as observed in the detailed XRD study, will be presented and compared to the single-solvent (CB) film to determine the optimum temperature.

XRD maps of the 1 : 11 CB–AN samples collected after annealing at different temperatures are shown in Fig. 5. Strong evolution of the Bragg peak, which corresponds to the alternate layers of polythiophene backbones and alkyl side chains, is observed with increasing annealing temperature. The peak intensity increases with increasing temperature up to 130 °C, then decreases. However, the peak intensity in directions other than the perfect edge-on direction (clearly visible from the 3D log scale presentation) increases gradually. To better understand the film structure, XRD profiles along the specular ($\Delta\theta \approx 0$) and off-specular ($\Delta\theta \approx 0.03°$) directions and rocking curves (around $2\theta \approx 3.4°$) for the as-cast, 130 °C-annealed and 165 °C-annealed mixed-solvent samples are plotted in Fig. 6. The XRD profiles and rocking curves for the as-cast, 130 °C-annealed and 165 °C-annealed single-solvent samples are also plotted in Fig. 6 for comparison. A large difference is observed between the mixed-solvent and single-solvent as-cast films. The peaks that are present in the XRD curves for the mixed-solvent film along both the specular and off-specular directions are almost absent or broad for the single-solvent film. The nature of the changes in the structure of the film with annealing is similar for both films. However, the amount of change is different. Also, the broad hump is still present around the peak in the single-solvent film after annealing.

To get detailed quantitative information about the crystallinity of the films, each XRD curve around the peak was fitted

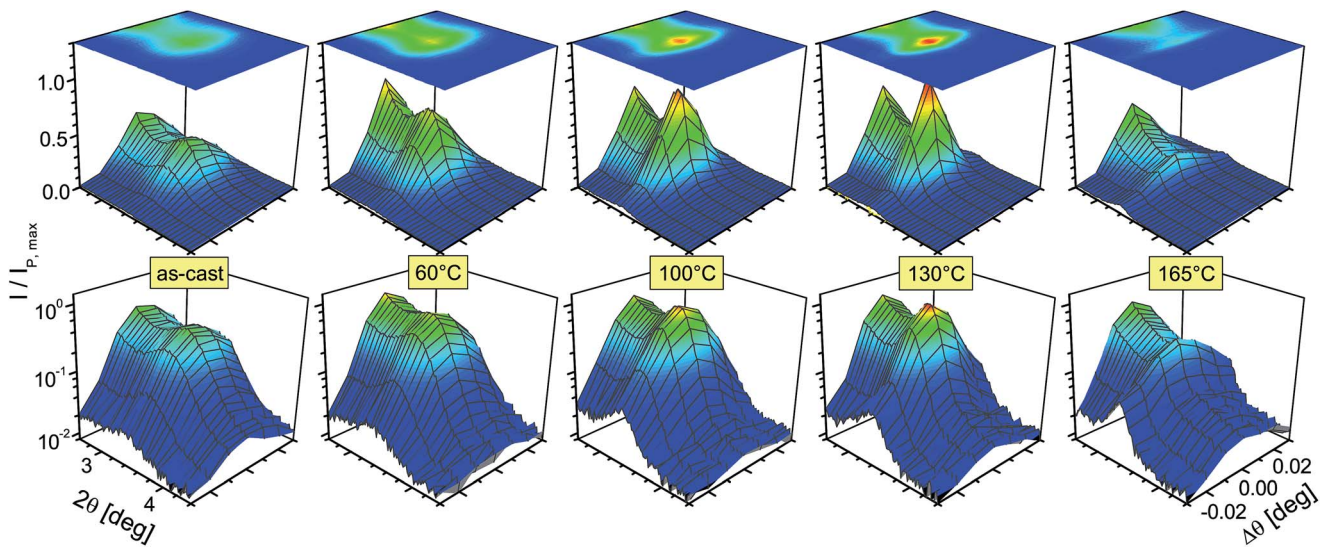

Fig. 5 XRD maps of the as-cast and different-temperature-annealed 1 : 11 CB–AN P3DDT films, showing the evolution of the Bragg peak, which corresponds to the alternate layers of polythiophene backbones and alkyl side chains, in three modes of presentation.

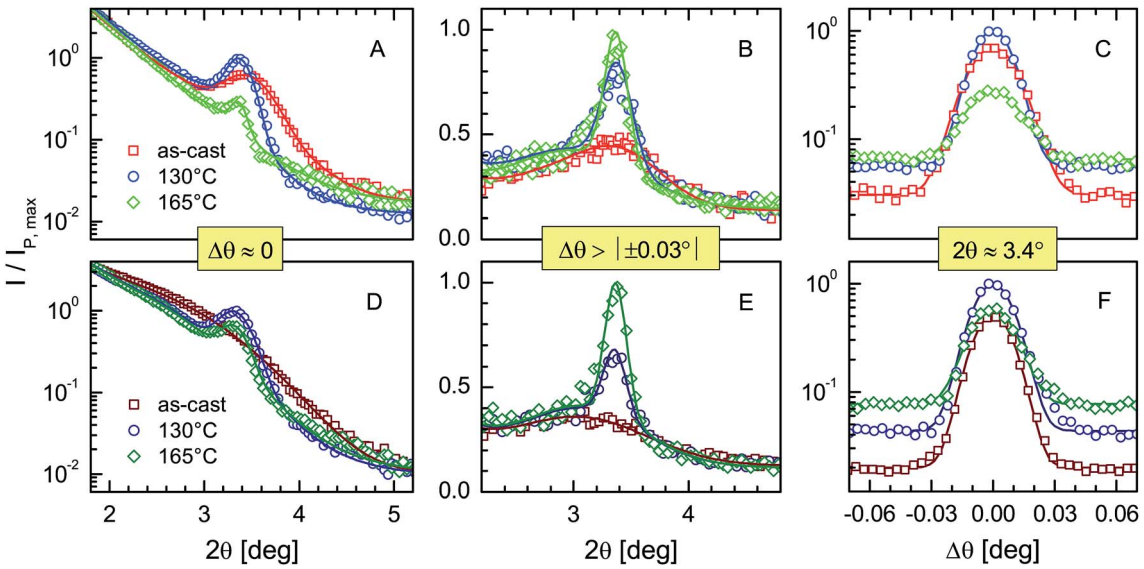

Fig. 6 XRD profiles (along the specular, $\Delta\theta \approx 0$, and off-specular, $\Delta\theta \approx 0.03°$, directions) and rocking curves (around $2\theta \approx 3.4°$) for the as-cast, 130 °C-annealed and 165 °C-annealed P3DDT films. A, B and C are for the mixed-solvent (1 : 11 CB–AN) films; D, E and F are for the single-solvent (CB) films.

with a single or double Gaussian peak(s) along with an exponentially decreasing background, as before. The variation in the size and amount of crystallites with annealing temperature along the specular and off-specular directions for the mixed- and single-solvent films is shown in Fig. 7. The increase in the size of the crystallites with increasing annealing temperature is clearly visible. For the mixed-solvent film, two different sizes of crystallites are observed. Along the specular direction, the ~6 and 15 nm crystallites for the as-cast film increase gradually to ~20 and 44 nm, respectively, after annealing, while along the off-specular direction, the ~6 nm size crystallites for the as-cast film remain almost the same size and the ~10 nm size crystallites increase gradually to ~34 nm after annealing. The intensity or amount of the nanocrystallites along the specular direction, which is quite high initially, further increases (or remains almost the same) up to an annealing temperature of 130 °C and then decreases considerably, while the intensity along the off-specular direction, which is quite low initially, increases gradually with increasing annealing temperature. It can be noted that the XRD and GISAXS results for the different poor-solvent films presented before are somewhat of an average of the results along the specular and off-specular directions, which is expected. As for the XRD measurements of the different poor-solvent films, no special alignments have been made, which are required for estimation along the specular direction. Also for the GISAXS measurements, the Bragg peak at $q_y = 0$ has some non-zero q_x component (as the incident angle is $\leq 0.4°$ and the exit angle is $\geq 1.6°$ for $2\theta_B \approx 2°$). For the as-cast single-solvent film, no crystallite is observed initially along the specular direction, while very low intensity, very small (~6 nm) size crystallites are observed along the off-specular direction. After annealing the film, crystallites about 20–25 nm in size are formed along the specular direction, while crystallites ~35 nm in size are formed additionally along the off-specular direction. The intensity along the specular direction is quite high compared to the off-specular direction. Also the intensity along the specular direction is greatest around 130 °C, while that along the off-specular direction increases gradually, similar to

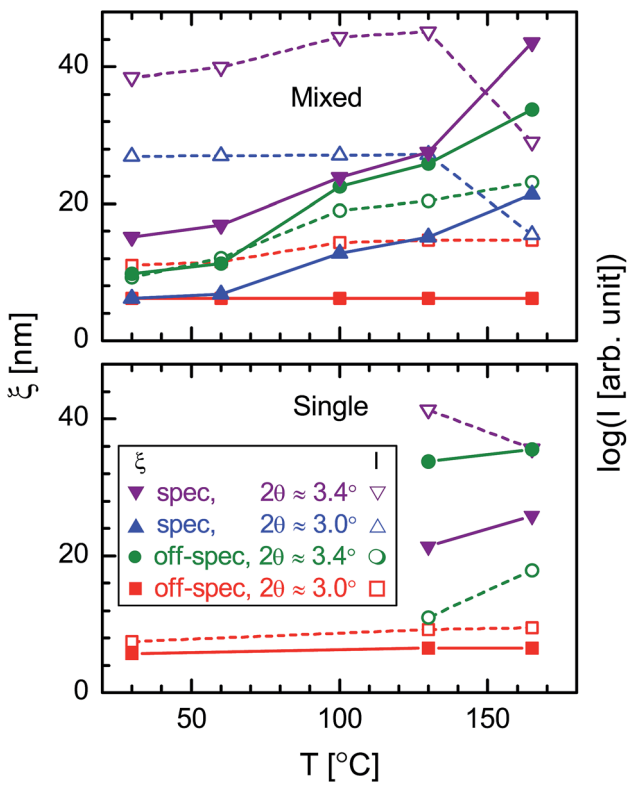

Fig. 7 Variation of the crystallite-size (ξ) and intensity (I) with annealing temperature along the specular and off-specular directions for the mixed- and single-solvent films.

This journal is © The Royal Society of Chemistry 2015

the mixed-solvent film. Relatively large size crystallites and their normalized amount along the specular and off-specular directions for the as-cast, 130 °C-annealed and 165 °C-annealed mixed- and single-solvent P3DDT films are also tabulated in Table 2.

So far we have used different films for annealing at different temperatures to understand the structure. We will now cross check it with a single film annealed at different temperatures. For that, XRD data of a single 1 : 11 CB–AN film on quartz glass, collected after annealing at different temperatures, are plotted in Fig. 8. The crystallites' size (ξ) and their normalized amount (f), obtained from the peak of each XRD data (as before), are plotted as a function of the annealing temperature in the insets of Fig. 8. A considerable increase in the size of the crystallites is observed for annealing above 100 °C, the amount of which increases significantly up to 130 °C and then decreases, as before. So, XRD analysis of all the P3DDT films clearly suggests that the optimum annealing temperature is around 130 °C.

3.2 Structure from atomic force microscopy

Typical AFM images of the as-cast, 130 °C-annealed and 165 °C-annealed 1 : 11 CB–AN P3DDT films, are shown in Fig. 9 in two length scales. Island-like structures on the P3DDT films are evident from the large scale (5 μm × 5 μm) topographic images. The size of the islands is found to be in the range of 0.6–0.8 μm, and remains almost unaffected after annealing. The height of the islands, which is about 130 nm for the as-cast film, decreases gradually to about 100 nm for the 130 °C-annealed film and to about 80 nm for the 165 °C-annealed film. The island-like structure is, however, composed of small domain-like structures, which are clearly evident from the small scale (0.5 μm × 0.5 μm) topographic images. The size of the domains is about 50 ± 10 nm for the as-cast film, increasing slightly to about 60 ± 10 nm for the 130 °C-annealed film and then decreasing slightly to about 45 ± 10 nm for the 165 °C-annealed film. The height of the compact domains can not be resolved from the images, although the maximum height variation (z_m) within the scan size is found to decrease with increasing annealing temperature.

Table 2 Parameters such as relatively large size crystallites (ξ) and normalized amount (f) along the specular (s) and off-specular (os) directions for the as-cast, 130 °C and 165 °C-annealed mixed-solvent (1 : 11 CB–AN) and single-solvent (CB) P3DDT films

Annealing temperature	Mixed-solvent film				Single-solvent film			
	ξ_s (nm)	f_s	ξ_{os} (nm)	f_{os}	ξ_s (nm)	f_s	ξ_{os} (nm)	f_{os}
As-cast	15	0.4	10	0.2	—	—	—	—
130 °C	28	0.9	26	0.5	21	1.0	34	0.3
165 °C	44	0.2	34	0.7	26	0.6	36	0.7

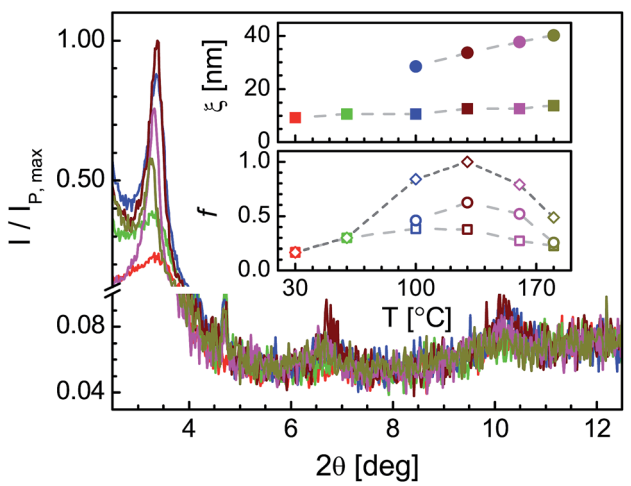

Fig. 8 XRD curves of an as-cast 1 : 11 CB–AN P3DDT film on quartz glass and after annealing at different temperatures, showing the evolution of Bragg peaks, which corresponds to the alternate layers of polythiophene backbones and alkyl side chains. Insets: corresponding variation of crystallites' size (ξ) and relative amount (f) with annealing temperature.

3.3 Structure from optical spectroscopy

The UV-vis absorption spectra of the 1 : 11 CB–AN films on quartz glass substrates, collected after annealing at different temperatures, are shown in Fig. 10. Four shoulders/peaks at about 490, 530, 560 and 610 nm are visible in all the curves. The appearance of the well-resolved peaks is mainly due to π–π stacking. The absorption peak at around 610 nm originates from the interchain π–π transition, while the absorption peaks at 560, 530 and 490 nm are attributed to the 0–0, 0–1 and 0–2 transitions of the intrachain exciton.[39] The peak at about 490 nm can also appear due to the intrachain π–π transition of the planar rod-like conformation of the P3AT chains, which is at about 450 nm for the coil-like conformation of the P3AT chains comprising twisting and bending of the thiophene rings. The observed spectral signatures can also be described using weakly interacting H-aggregates, where the intensity ratio (A_1/A_2) of the peaks at 610 and 560 nm can be used to extract the free exciton bandwidth of the aggregates, which is related to the coupling strength and conjugation length.[40]

There is almost no peak near 450 nm, indicating that very few chains in the coil-like conformation are present in the film. The intense peak at around 490 nm for the as-cast film indicates the presence of a large amount of non-interacting chains in the rod-like conformation. The further increase of that peak for the 60 °C-annealed film indicates the increased presence of rod-like chains. The intensity of that peak, however, decreases gradually after annealing above 100 °C, suggesting a decrease in the amount of free rod-like chains due to the ordering of the rod-like chains to form lamellae or H-aggregates, as is evident from the gradual increase in peak intensity at around 560 and 610 nm. For the as-cast film and the films annealed at temperatures up to 130 °C, there is very little change in the ratio A_1/A_2, suggesting very little change in the conjugation length. This indicates that the enhancement of lamellae size is predominantly along the alkyl side chain direction. For the film annealed at 165 °C, there is a small increase in the A_1/A_2 ratio and a slight blue shift of the corresponding peaks. The

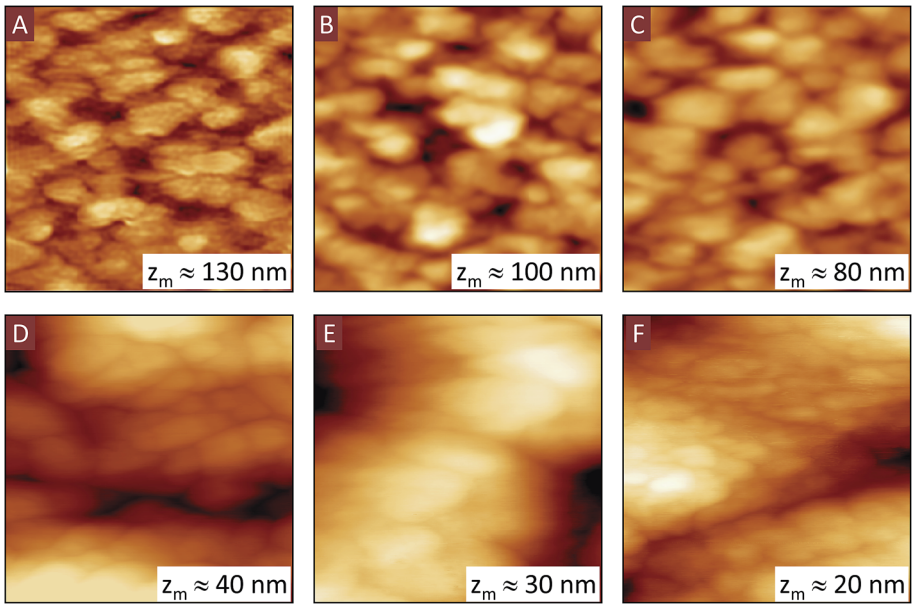

Fig. 9 Typical AFM images in two length scales (A, B and C for scan size: 5 μm × 5 μm and D, E and F for scan size: 0.5 μm × 0.5 μm) showing the topography of the as-cast (A and D), 130 °C (B and E) and 165 °C (C and F) annealed 1 : 11 CB–AN P3DDT films. z_m indicates the maximum height variation.

combination of both probably indicates some kind of change in the structure or orientation of the lamellae.

To better understand the effect of poor solvent on the structure of the P3DDT molecules, UV-vis spectra of the solutions of P3DDT in single (CB) and mixed (CB–AN) solvents, collected after 4 h of mixing, are shown in Fig. 11. A peak near 450 nm is observed in the spectrum of the single-solvent solution, indicating the presence of molecules in the coil-like conformation, while that peak is shifted towards higher wavelength in the mixed-solvent spectrum suggesting that predominantly molecules in the rod-like conformation are present. Peaks near 530, 560 and 610 nm are also visible in the spectrum of mixed solution, similar to those of the 1 : 11 CB–AN films, suggesting the formation of some P3DDT aggregates in the solution within 4 h.

3.4 Structure from dynamic light scattering

Intensity particle size distribution curves, obtained from the DLS measurements, for the solutions of P3DDT in single (CB) and mixed (CB–AN) solvents, collected after 4 h of mixing, are shown in Fig. 12. A single peak is observed in the curve for the single solution, while two peaks are observed in the curve for the mixed solution. The size obtained from the single solution

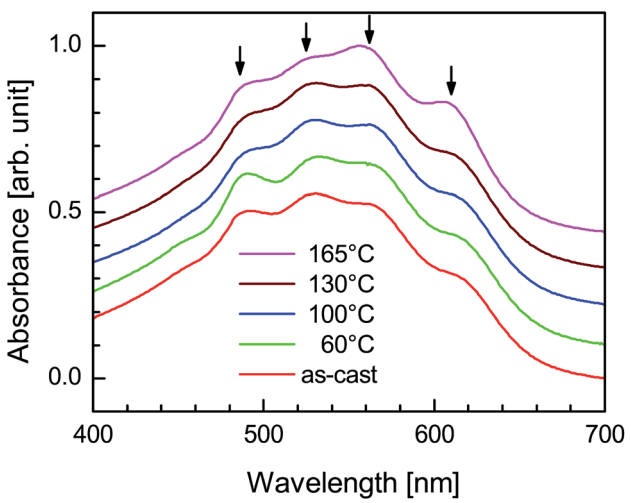

Fig. 10 UV-vis spectra of the as-cast and different-temperature-annealed 1 : 11 CB–AN P3DDT films on glass substrates. Peak positions are indicated by arrows.

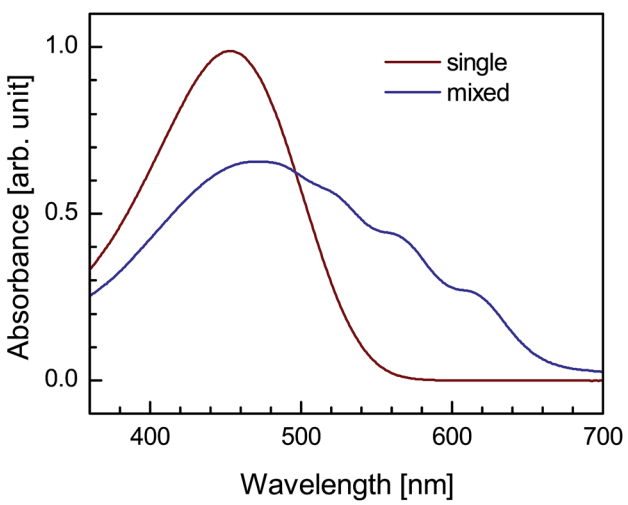

Fig. 11 UV-vis spectra for the solutions of P3DDT in single (good) and mixed (good and poor) solvents, collected after 4 h of mixing.

This journal is © The Royal Society of Chemistry 2015

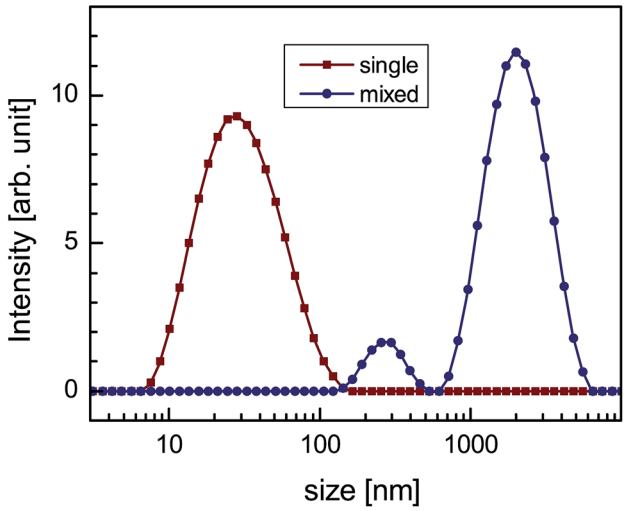

Fig. 12 Intensity particle size distribution curves obtained from the DLS measurements for the solutions of P3DDT in single (good) and mixed (good and poor) solvents, collected after 4 h of mixing.

is about 27 nm, which can be attributed to the average hydrodynamic diameter of the P3DDT when the chains are in the coil-like configuration. The sizes obtained from the mixed solution are about 270 and 2000 nm. The former can be attributed to the average hydrodynamic diameter of the P3DDT when chains are in the rod-like configuration, while the latter probably corresponds to the size of the aggregates.

3.5 Structures of the P3DDT films and growth mechanism

The structures of the P3DDT films deposited from different good solvent to poor solvent ratios without thermal annealing (*i.e.* as-cast) and after subsequent annealing at different temperatures, obtained from the analysis of the complementary data, are shown schematically in Fig. 13. In general, the P3DDT films are composed of coil-like and rod-like chains and lamellar

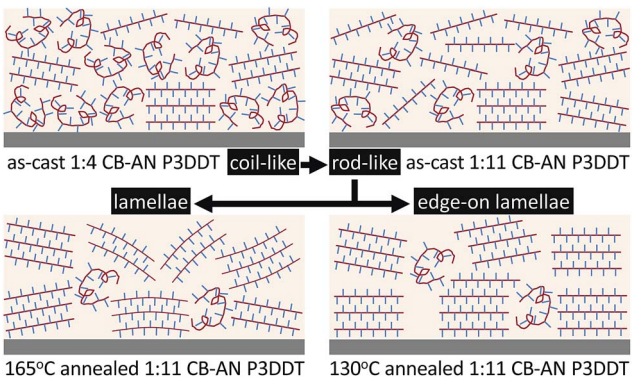

Fig. 13 Schematic illustration of the structures of the P3DDT films showing the increased prevalence of rod-like conformations with poor solvent (for as-cast films), the enhancement of lamellae structures (due to subsequent ordering of such rods) with increasing annealing temperature (for the 1 : 11 CB–AN films) and the particular enhancement of the edge-on oriented lamellae near 130 °C.

crystallites. For the as-cast 1 : 4 CB–AN film, the coil-like chains are more prevalent compared to the rod-like chains, while for the as-cast 1 : 11 CB–AN film, the rod-like chains are much more prevalent compared to the coil-like chains. Also, a few small sized lamellar crystallites are present in both the films. For the 60 °C-annealed film, the amount of rod-like chains increases, while the amount of coil-like chains decreases. For the films annealed above 100 °C, the amount of free rod-like chains also decreases, while the amount and size of the crystallites increases. For the 130 °C-annealed 1 : 11 CB–AN film, the amount and/or size of the highly edge-on oriented lamellar crystallites is found to be the greatest, while for the 165 °C-annealed film the orientation of the crystallites becomes random.

It is known that P3AT crystallization evolves in two steps, namely, the coil-to-rod conformational transition followed by the organization of the rod-like chains through strong anisotropic π–π interactions between their planar rigid backbones and weak van der Waals interactions between their pendent alkyl side chains.[41–43] In a good solvent, P3DDT dissolves well to form a near-equilibrium homogeneous system.[26] This solution mostly consists of coil-like polymer chains, which are energetically favorable and also clearly evident from both optical absorption and DLS measurements. Addition of a poor solvent makes the solution inhomogeneous and disturbs the equilibrium. Polymers, which are in contact with the poor solvent, experience different polymer–solvent interaction, resulting in a coil-to-rod conformational transition. This is also quite evident from the optical absorption and DLS measurements.[44] Accordingly, the prevalence of the rod conformation increases with the increase of poor solvent. Also aggregates, which are a mixture of crystal and amorphous, are formed during this stage (see DLS measurement) and appeared as domains in the film (see AFM images). However, only small amount of rods are organized to form crystallites (which are sensitive to the optical absorption and XRD measurements) in the solution and in the as-cast films, prepared after aging and normal drying. This indicates that the poor solvent is mainly inducing the unfavorable coil-to-rod conformational transition (negative entropy change) and acting very little on the further unfavorable π–π stacking (which also requires a negative entropy change). Thermal annealing seems to be responsible for the π–π stacking. For the present P3DDT polymer, melting of the alkyl side chains takes place in the temperature range 50–80 °C, while melting of the polythiophene backbones takes place in the temperature range 150–170 °C (see Fig. S2†). Thus annealing above the first temperature range sets the rod-like polymer chains free and promotes diffusion. Also the thermal energy essentially helps to overcome the unfavorable π–π stacking condition. Increasing the annealing temperature increases the π–π stacking. Organization of the π–π stacked layers through the alkyl side chains then initiates to lower the energy. Subsequent cooling predominantly forms edge-on oriented crystallites. Room temperature, on the other hand can only induce limited π–π stacking, hence only small crystallites are observed in the as-cast films. Alkyl side chains in such crystallites are slightly interpenetrating and strained (Form-II like), but upon annealing become more

relaxed (Form-I like). Annealing the film near the second temperature range twists and deforms the rod-like polymer chains. This effect increases with increasing annealing temperature. Accordingly, more deformed and fewer edge-on oriented crystallites are formed upon subsequent cooling. It is necessary to mention that the thermal energy helps not only to overcome the unfavorable π–π stacking condition but also to overcome the unfavorable coil-to-rod conformational transition. This is clearly evident for the P3DDT films prepared from a single solvent, the crystallites of which increase with thermal annealing. However, the thermal annealing along with the initial poor-solvent effect in the mixed-solvent films enhanced the overall coil-to-rod conformational transition and the formation of crystallites. This enhancement with thermal annealing is essentially restricted within small-size domains that are formed in the as-cast film (since not much change in the domain size is observed from AFM).

4 Conclusions

We have shown that P3DDT films with predominantly edge-on oriented lamellae can be prepared by a simple drop-casting method from its solutions in a mixture of a good and a poor solvent, namely, chlorobenzene and anisole, and subsequent thermal annealing of the films. These lamellae are restricted within small domains (~50 nm) and nearly isotropic in shape. The degree of crystallinity in the annealed films can be enhanced by increasing the proportion of poor solvent in the solution, as is evident from the XRD and GISAXS patterns. Annealing beyond the melting temperature of the alkyl side chains and below that of the polythiophene backbone brings about an increase in directionality of the lamellae, whereas annealing directly above the melting temperature of the backbone results in increased crystallinity at the cost of decreased directionality, as is clearly evident from the XRD maps. The XRD data of the films cast on hydrophobic H-passivated Si and hydrophilic oxide-covered Si show a similar nature for both the as-cast and annealed films. A similar nature is also observed for films cast on H-passivated Si(001) and Si(111). This means that the P3DDT molecules adopt an edge-on orientation irrespective of the nature of the substrate. The combination of XRD and UV-vis measurements clearly shows that the rod-to-coil conformational transition mainly takes place due to the addition of the poor solvent to the solution, while organization of the rod-like chains takes place due to the subsequent thermal annealing of the film. Annealing beyond the melting temperature of the alkyl side chains helps to form well-ordered edge-on oriented P3DDT lamellae structures, which degrade when the melting temperature of the polythiophene backbone is reached. The optimal annealing temperature for producing well-ordered edge-on oriented P3DDT lamellae was found to be around 130 °C. So the degree of crystallinity and directionality of the semicrystalline polymer P3DDT, which is of immense importance in its performance as a semiconducting material, can be well regulated by varying the good solvent to poor solvent ratio and by choosing the proper temperature for post-deposition annealing.

Acknowledgements

The authors thank Dr S. V. Roth for his support in GISAXS measurements, Prof. P. M. G. Nambissan and Ms Soma Roy for their help in UV-vis measurements and Prof. M. Mukherjee for providing DLS facilities. The financial support received from the Saha Institute of Nuclear Physics under the DST-DESY project to carry out GISAXS experiments at PETRA III is thankfully acknowledged.

References

1 J. H. Burroughes, D. D. C. Bradley, A. R. Brown, R. N. Marks, K. Mackay, R. H. Friend, P. L. Burns and A. B. Holmes, *Nature*, 1990, **347**, 539.
2 M. Berggren, O. Inganas, G. Gustafsson, J. Rasmusson, M. R. Andersson, T. Hjertberg and O. Wennerstrom, *Nature*, 1994, **372**, 444.
3 G. Yu, J. Gao, J. C. Hummelen, F. Wudl and A. J. Heeger, *Science*, 1995, **270**, 1789.
4 Y. Liang, Z. Xu, J. Xia, S.-T. Tsai, Y. Wu, G. Li, C. Ray and L. Yu, *Adv. Mater.*, 2010, **22**, E135.
5 L. Qiu, W. H. Lee, X. Wang, J. S. Kim, J. A. Lim, D. Kwak, S. Lee and K. Cho, *Adv. Mater.*, 2009, **21**, 1349.
6 H. Yan, Z. Chen, Y. Zheng, C. Newman, J. R. Quinn, F. Dotz, M. Kastler and A. Facchetti, *Nature*, 2009, **457**, 679.
7 H. Sirringhaus, P. J. Brown, R. H. Friend, M. M. Nielsen, K. Bechgaard, B. M. W. Langeveld-Voss, A. J. H. Spiering, R. A. J. Janssen, E. W. Meijer, P. Herwig and D. M. de Leeuw, *Nature*, 1999, **401**, 685.
8 X. Shen, V. V. Duzhko and T. P. Russell, *Adv. Energy Mater.*, 2013, **3**, 263.
9 K.-Y. Jen, G. G. Miller and R. L. Elsenbaumer, *J. Chem. Soc., Chem. Commun.*, 1986, **17**, 1346.
10 R. L. Elsenbaumer, K.-Y. Jen and R. Oboodi, *Synth. Met.*, 1986, **15**, 169.
11 S. Hotta, S. D. D. V. Rughooputh, A. J. Heeger and F. Wudl, *Macromolecules*, 1987, **20**, 212.
12 S. T. Shabi, E. Mikayelyan, S. Grigorian, U. Pietsch, N. Koenen, U. Scherf, N. Kayunkid and M. Brinkmann, *Macromolecules*, 2012, **45**, 5575.
13 R. J. Kline, M. D. McGehee, E. N. Kadnikova, J. Liu and J. M. J. Frechet, *Adv. Mater.*, 2003, **15**, 1519.
14 V. Causin, C. Marega, A. Marigo, L. Valentini and J. M. Kenny, *Macromolecules*, 2005, **38**, 409.
15 J.-F. Chang, B. Sun, D. W. Breiby, M. M. Nielsen, T. I. Solling, M. Giles, I. McCulloch and H. Sirringhaus, *Chem. Mater.*, 2004, **16**, 4772.
16 R. J. Kline, M. D. McGehee and M. F. Toney, *Nat. Mater.*, 2006, **5**, 222.
17 M. Brinkmann and J.-C. Wittmann, *Adv. Mater.*, 2006, **18**, 860.
18 H. Yang, S. W. LeFevre, C. Y. Ryu and Z. Bao, *Appl. Phys. Lett.*, 2007, **90**, 172116.
19 A. Salleo, R. J. Kline, D. M. DeLongchamp and M. L. Chabinyc, *Adv. Mater.*, 2010, **22**, 3812.

 This journal is © The Royal Society of Chemistry 2015

20 S. T. Shabi, S. Grigorian, M. Brinkmann, U. Pietsch, N. Koenen, N. Kayunkid and U. Scherf, *J. Appl. Polym. Sci.*, 2012, **125**, 2335.
21 Y. Fu, C. Lin and F.-Y. Tsai, *Org. Electron.*, 2009, **10**, 883.
22 N. Kiriy, E. Jahne, H.-J. Adler, M. Schneider, A. Kiriy, G. Gorodyska, S. Minko, D. Jehnichen, P. Simon, A. A. Fokin and M. Stamm, *Nano Lett.*, 2003, **3**, 707.
23 Y. D. Park, H. S. Lee, Y. J. Choi, D. Kwak, J. H. Cho, S. Lee and K. Cho, *Adv. Funct. Mater.*, 2009, **19**, 1200.
24 Z. Yu, H. Yan, K. Lu, Y. Zhang and Z. Wei, *RSC Adv.*, 2012, **2**, 338.
25 M. Chang, D. Choi, B. Fu and E. Reichmanis, *ACS Nano*, 2013, **7**, 5402.
26 W. Xu, L. Li, H. Tang, H. Li, X. Zhao and X. Yang, *J. Phys. Chem. B*, 2011, **115**, 6412.
27 H. F. Okorn-Schmidt, *IBM J. Res. Dev.*, 1999, **43**, 351.
28 X. G. Zhang, *Electrochemistry of Silicon and its Oxide*, Kluwer Academic, New York, 2004.
29 J. K. Bal and S. Hazra, *Phys. Rev. B: Condens. Matter Mater. Phys.*, 2007, **75**, 205411.
30 P. Chatterjee, S. Hazra and H. Amenitsch, *Soft Matter*, 2012, **8**, 2956.
31 S. Hazra, *Appl. Surf. Sci.*, 2006, **253**, 2154.
32 J. K. Bal and S. Hazra, *Phys. Rev. B: Condens. Matter Mater. Phys.*, 2009, **79**, 155405.
33 J. K. Bal and S. Hazra, *Phys. Rev. B: Condens. Matter Mater. Phys.*, 2009, **79**, 155412.
34 S. V. Roth, G. Herzog, V. Körstgens, A. Buffet, M. Schwartzkopf, J. Perlich, M. M. A. Kashem, R. Döhrmann, R. Gehrke, A. Rothkirch, K. Stassig, W. Wurth, G. Benecke, C. Li, P. Fratzl, M. Rawolle and P. Müller-Buschbaum, *J. Phys.: Condens. Matter*, 2011, **23**, 254208.
35 P. Chatterjee and S. Hazra, *Soft Matter*, 2013, **9**, 9799.
36 P. Chatterjee and S. Hazra, *J. Phys. Chem. C*, 2014, **118**, 11350.
37 K. Yazawa, Y. Inoue, T. Yamamoto and N. Asakawa, *Phys. Rev. B: Condens. Matter Mater. Phys.*, 2006, **74**, 094204.
38 Y. Guo, Y. Jin and Z. Su, *Soft Matter*, 2012, **8**, 2907.
39 P. J. Brown, D. S. Thomas, A. Kohler, J. S. Wilson, J.-S. Kim, C. M. Ramsdale, H. Sirringhaus and R. H. Friend, *Phys. Rev. B: Condens. Matter Mater. Phys.*, 2003, **67**, 064203.
40 J. Clark, C. Silva, R. H. Friend and F. C. Spano, *Phys. Rev. Lett.*, 2007, **98**, 206406.
41 S. Malik and A. K. Nandi, *J. Polym. Sci., Part B: Polym. Phys.*, 2002, **40**, 2073.
42 Y. Takizawa, T. Shimomura and T. Miura, *J. Phys. Chem. B*, 2013, **117**, 6282.
43 W. Dierckx, W. D. Oosterbaan, J.-C. Bolsee, W. Maes, D. Vanderzande and J. Manca, *J. Mater. Chem. C*, 2014, **2**, 5730.
44 J. Liu, S. Shao, H. Wang, K. Zhao, L. Xue, X. Gao, Z. Xie and Y. Han, *Org. Electron.*, 2010, **11**, 775.